Old Dominion University
ODU Digital Commons

Physics Faculty Publications   Physics

2013

Experimental Studies of Di-Jets in Au + Au Collisions Using Angular Correlations With Respect to Back-to-Back Leading Hadrons

L. Adamczyk

G. Agakishiev

M. M. Aggarwal

Z. Ahammed

I. Koralt
Old Dominion University

See next page for additional authors

Follow this and additional works at: https://digitalcommons.odu.edu/physics_fac_pubs

Part of the Nuclear Commons

Authors

L. Adamczyk, G. Agakishiev, M. M. Aggarwal, Z. Ahammed, I. Koralt, and STAR Collaboration

Experimental studies of di-jets in Au + Au collisions using angular correlations with respect to back-to-back leading hadrons

L. Adamczyk,[1] G. Agakishiev,[21] M. M. Aggarwal,[34] Z. Ahammed,[53] A. V. Alakhverdyants,[21] I. Alekseev,[19] J. Alford,[22]
C. D. Anson,[31] D. Arkhipkin,[4] E. Aschenauer,[4] G. S. Averichev,[21] J. Balewski,[26] A. Banerjee,[53] Z. Barnovska,[14]
D. R. Beavis,[4] R. Bellwied,[49] M. J. Betancourt,[26] R. R. Betts,[10] A. Bhasin,[20] A. K. Bhati,[34] H. Bichsel,[55] J. Bielcik,[13]
J. Bielcikova,[14] L. C. Bland,[4] I. G. Bordyuzhin,[19] W. Borowski,[45] J. Bouchet,[22] A. V. Brandin,[29] S. G. Brovko,[6] E. Bruna,[57]
S. Bültmann,[32] I. Bunzarov,[21] T. P. Burton,[4] J. Butterworth,[40] X. Z. Cai,[44] H. Caines,[57] M. Calderón de la Barca Sánchez,[6]
D. Cebra,[6] R. Cendejas,[7] M. C. Cervantes,[47] P. Chaloupka,[13] Z. Chang,[47] S. Chattopadhyay,[53] H. F. Chen,[42] J. H. Chen,[44]
J. Y. Chen,[9] L. Chen,[9] J. Cheng,[50] M. Cherney,[12] A. Chikanian,[57] W. Christie,[4] P. Chung,[14] J. Chwastowski,[11]
M. J. M. Codrington,[47] R. Corliss,[26] J. G. Cramer,[55] H. J. Crawford,[5] X. Cui,[42] S. Das,[16] A. Davila Leyva,[48] L. C. De Silva,[49]
R. R. Debbe,[4] T. G. Dedovich,[21] J. Deng,[43] R. Derradi de Souza,[8] S. Dhamija,[18] L. Didenko,[4] F. Ding,[6] A. Dion,[4]
P. Djawotho,[47] X. Dong,[25] J. L. Drachenberg,[47] J. E. Draper,[6] C. M. Du,[24] L. E. Dunkelberger,[7] J. C. Dunlop,[4] L. G. Efimov,[21]
M. Elnimr,[56] J. Engelage,[5] G. Eppley,[40] L. Eun,[25] O. Evdokimov,[10] R. Fatemi,[23] S. Fazio,[4] J. Fedorisin,[21] R. G. Fersch,[23]
P. Filip,[21] E. Finch,[57] Y. Fisyak,[4] C. A. Gagliardi,[47] D. R. Gangadharan,[31] F. Geurts,[40] A. Gibson,[52] S. Gliske,[2]
Y. N. Gorbunov,[12] O. G. Grebenyuk,[25] D. Grosnick,[52] S. Gupta,[20] W. Guryn,[4] B. Haag,[6] O. Hajkova,[13] A. Hamed,[47]
L-X. Han,[44] J. W. Harris,[57] J. P. Hays-Wehle,[26] S. Heppelmann,[35] A. Hirsch,[37] G. W. Hoffmann,[48] D. J. Hofman,[10] S. Horvat,[57]
B. Huang,[4] H. Z. Huang,[7] P. Huck,[9] T. J. Humanic,[31] L. Huo,[47] G. Igo,[7] W. W. Jacobs,[18] C. Jena,[30] E. G. Judd,[5] S. Kabana,[45]
K. Kang,[50] J. Kapitan,[14] K. Kauder,[10] H. W. Ke,[9] D. Keane,[22] A. Kechechyan,[21] A. Kesich,[6] D. P. Kikola,[37] J. Kiryluk,[25]
I. Kisel,[25] A. Kisiel,[54] V. Kizka,[21] S. R. Klein,[25] D. D. Koetke,[52] T. Kollegger,[15] J. Konzer,[37] I. Koralt,[32] L. Koroleva,[19]
W. Korsch,[23] L. Kotchenda,[29] P. Kravtsov,[29] K. Krueger,[2] I. Kulakov,[25] L. Kumar,[22] M. A. C. Lamont,[4] J. M. Landgraf,[4]
S. LaPointe,[56] J. Lauret,[4] A. Lebedev,[4] R. Lednicky,[21] J. H. Lee,[4] W. Leight,[26] M. J. LeVine,[4] C. Li,[42] L. Li,[48] W. Li,[44] X. Li,[37]
X. Li,[46] Y. Li,[50] Z. M. Li,[9] L. M. Lima,[41] M. A. Lisa,[31] F. Liu,[9] T. Ljubicic,[4] W. J. Llope,[40] R. S. Longacre,[4] Y. Lu,[42] X. Luo,[9]
A. Luszczak,[11] G. L. Ma,[44] Y. G. Ma,[44] D. M. M. D. Madagodagettige Don,[12] D. P. Mahapatra,[16] R. Majka,[57] O. I. Mall,[6]
S. Margetis,[22] C. Markert,[48] H. Masui,[25] H. S. Matis,[25] D. McDonald,[40] T. S. McShane,[12] S. Mioduszewski,[47]
M. K. Mitrovski,[4] Y. Mohammed,[47] B. Mohanty,[30] M. M. Mondal,[47] B. Morozov,[19] M. G. Munhoz,[41] M. K. Mustafa,[37]
M. Naglis,[25] B. K. Nandi,[17] Md. Nasim,[53] T. K. Nayak,[53] J. M. Nelson,[3] L. V. Nogach,[36] J. Novak,[28] G. Odyniec,[25] A. Ogawa,[4]
K. Oh,[38] A. Ohlson,[57] V. Okorokov,[29] E. W. Oldag,[48] R. A. N. Oliveira,[41] D. Olson,[25] P. Ostrowski,[54] M. Pachr,[13] B. S. Page,[18]
S. K. Pal,[53] Y. X. Pan,[7] Y. Pandit,[22] Y. Panebratsev,[21] T. Pawlak,[54] B. Pawlik,[33] H. Pei,[10] C. Perkins,[5] W. Peryt,[54] P. Pile,[4]
M. Planinic,[58] J. Pluta,[54] D. Plyku,[32] N. Poljak,[58] J. Porter,[25] A. M. Poskanzer,[25] C. B. Powell,[25] C. Pruneau,[56] N. K. Pruthi,[34]
M. Przybycien,[1] P. R. Pujahari,[17] J. Putschke,[56] H. Qiu,[25] R. Raniwala,[39] S. Raniwala,[39] R. L. Ray,[48] R. Redwine,[26] R. Reed,[6]
C. K. Riley,[57] H. G. Ritter,[25] J. B. Roberts,[40] O. V. Rogachevskiy,[21] J. L. Romero,[6] J. F. Ross,[12] L. Ruan,[4] J. Rusnak,[14]
N. R. Sahoo,[53] P. K. Sahu,[16] I. Sakrejda,[25] S. Salur,[25] J. Sandweiss,[57] E. Sangaline,[6] A. Sarkar,[17] J. Schambach,[48]
R. P. Scharenberg,[37] A. M. Schmah,[25] B. Schmidke,[4] N. Schmitz,[27] T. R. Schuster,[15] J. Seele,[26] J. Seger,[12] P. Seyboth,[27]
N. Shah,[7] E. Shahaliev,[21] M. Shao,[42] B. Sharma,[34] M. Sharma,[56] S. S. Shi,[9] Q. Y. Shou,[44] E. P. Sichtermann,[25]
R. N. Singaraju,[53] M. J. Skoby,[18] D. Smirnov,[4] N. Smirnov,[57] D. Solanki,[39] P. Sorensen,[4] U. G. deSouza,[41] H. M. Spinka,[2]
B. Srivastava,[37] T. D. S. Stanislaus,[52] S. G. Steadman,[26] J. R. Stevens,[18] R. Stock,[15] M. Strikhanov,[29] B. Stringfellow,[37]
A. A. P. Suaide,[41] M. C. Suarez,[10] M. Sumbera,[14] X. M. Sun,[25] Y. Sun,[42] Z. Sun,[24] B. Surrow,[46] D. N. Svirida,[19]
T. J. M. Symons,[25] A. Szanto de Toledo,[41] J. Takahashi,[8] A. H. Tang,[4] Z. Tang,[42] L. H. Tarini,[56] T. Tarnowsky,[28] D. Thein,[48]
J. H. Thomas,[25] J. Tian,[44] A. R. Timmins,[49] D. Tlusty,[14] M. Tokarev,[21] S. Trentalange,[7] R. E. Tribble,[47] P. Tribedy,[53]
B. A. Trzeciak,[54] O. D. Tsai,[7] J. Turnau,[33] T. Ullrich,[4] D. G. Underwood,[2] G. Van Buren,[4] G. van Nieuwenhuizen,[26]
J. A. Vanfossen, Jr.,[22] R. Varma,[17] G. M. S. Vasconcelos,[8] F. Videbæk,[4] Y. P. Viyogi,[53] S. Vokal,[21] S. A. Voloshin,[56] A. Vossen,[18]
M. Wada,[48] F. Wang,[37] G. Wang,[7] H. Wang,[4] J. S. Wang,[24] Q. Wang,[37] X. L. Wang,[42] Y. Wang,[50] G. Webb,[23] J. C. Webb,[4]
G. D. Westfall,[28] C. Whitten, Jr.,[7] H. Wieman,[25] S. W. Wissink,[18] R. Witt,[51] W. Witzke,[23] Y. F. Wu,[9] Z. Xiao,[50] W. Xie,[37]
K. Xin,[40] H. Xu,[24] N. Xu,[25] Q. H. Xu,[43] W. Xu,[7] Y. Xu,[42] Z. Xu,[4] L. Xue,[44] Y. Yang,[24] Y. Yang,[9] P. Yepes,[40] Y. Yi,[37]
K. Yip,[4] I-K. Yoo,[38] M. Zawisza,[54] H. Zbroszczyk,[54] J. B. Zhang,[9] S. Zhang,[44] X. P. Zhang,[50] Y. Zhang,[42] Z. P. Zhang,[42]
F. Zhao,[7] J. Zhao,[44] C. Zhong,[44] X. Zhu,[50] Y. H. Zhu,[44] Y. Zoulkarneeva,[21] and M. Zyzak[25]

(STAR Collaboration)

[1]*AGH University of Science and Technology, Cracow, Poland*
[2]*Argonne National Laboratory, Argonne, Illinois 60439, USA*
[3]*University of Birmingham, Birmingham, United Kingdom*
[4]*Brookhaven National Laboratory, Upton, New York 11973, USA*
[5]*University of California, Berkeley, California 94720, USA*
[6]*University of California, Davis, California 95616, USA*
[7]*University of California, Los Angeles, California 90095, USA*
[8]*Universidade Estadual de Campinas, Sao Paulo, Brazil*
[9]*Central China Normal University (HZNU), Wuhan 430079, China*
[10]*University of Illinois at Chicago, Chicago, Illinois 60607, USA*

[11]*Cracow University of Technology, Cracow, Poland*
[12]*Creighton University, Omaha, Nebraska 68178, USA*
[13]*Czech Technical University in Prague, FNSPE, Prague, 115 19, Czech Republic*
[14]*Nuclear Physics Institute AS CR, 250 68 Řež/Prague, Czech Republic*
[15]*University of Frankfurt, Frankfurt, Germany*
[16]*Institute of Physics, Bhubaneswar 751005, India*
[17]*Indian Institute of Technology, Mumbai, India*
[18]*Indiana University, Bloomington, Indiana 47408, USA*
[19]*Alikhanov Institute for Theoretical and Experimental Physics, Moscow, Russia*
[20]*University of Jammu, Jammu 180001, India*
[21]*Joint Institute for Nuclear Research, Dubna 141 980, Russia*
[22]*Kent State University, Kent, Ohio 44242, USA*
[23]*University of Kentucky, Lexington, Kentucky 40506-0055, USA*
[24]*Institute of Modern Physics, Lanzhou, China*
[25]*Lawrence Berkeley National Laboratory, Berkeley, California 94720, USA*
[26]*Massachusetts Institute of Technology, Cambridge, Massachusetts 02139-4307, USA*
[27]*Max-Planck-Institut für Physik, Munich, Germany*
[28]*Michigan State University, East Lansing, Michigan 48824, USA*
[29]*Moscow Engineering Physics Institute, Moscow Russia*
[30]*National Institute of Science and Education and Research, Bhubaneswar 751005, India*
[31]*Ohio State University, Columbus, Ohio 43210, USA*
[32]*Old Dominion University, Norfolk, Virginia 23529, USA*
[33]*Institute of Nuclear Physics PAN, Cracow, Poland*
[34]*Panjab University, Chandigarh 160014, India*
[35]*Pennsylvania State University, University Park, Pennsylvania 16802, USA*
[36]*Institute of High Energy Physics, Protvino, Russia*
[37]*Purdue University, West Lafayette, Indiana 47907, USA*
[38]*Pusan National University, Pusan, Republic of Korea*
[39]*University of Rajasthan, Jaipur 302004, India*
[40]*Rice University, Houston, Texas 77251, USA*
[41]*Universidade de Sao Paulo, Sao Paulo, Brazil*
[42]*University of Science & Technology of China, Hefei 230026, China*
[43]*Shandong University, Jinan, Shandong 250100, China*
[44]*Shanghai Institute of Applied Physics, Shanghai 201800, China*
[45]*SUBATECH, Nantes, France*
[46]*Temple University, Philadelphia, Pennsylvania 19122, USA*
[47]*Texas A&M University, College Station, Texas 77843, USA*
[48]*University of Texas, Austin, Texas 78712, USA*
[49]*University of Houston, Houston, Texas 77204, USA*
[50]*Tsinghua University, Beijing 100084, China*
[51]*United States Naval Academy, Annapolis, Maryland 21402, USA*
[52]*Valparaiso University, Valparaiso, Indiana 46383, USA*
[53]*Variable Energy Cyclotron Centre, Kolkata 700064, India*
[54]*Warsaw University of Technology, Warsaw, Poland*
[55]*University of Washington, Seattle, Washington 98195, USA*
[56]*Wayne State University, Detroit, Michigan 48201, USA*
[57]*Yale University, New Haven, Connecticut 06520, USA*
[58]*University of Zagreb, Zagreb HR-10002, Croatia*

Jet-medium interactions are studied via a multihadron correlation technique (called "2 + 1"), where a pair of back-to-back hadron triggers with large transverse momentum is used as a proxy for a di-jet. This work extends the previous analysis for nearly symmetric trigger pairs with the highest momentum threshold of trigger hadron of 5 GeV/c with the new calorimeter-based triggers with energy thresholds of up to 10 GeV and above. The distributions of associated hadrons are studied in terms of correlation shapes and per-trigger yields on each trigger side. In contrast with di-hadron correlation results with single triggers, the associated hadron distributions for back-to-back triggers from central Au + Au data at $\sqrt{s_{NN}} = 200$ GeV show no strong modifications compared to d + Au data at the same energy. An imbalance in the total transverse momentum between hadrons attributed

to the near-side and away-side of jetlike peaks is observed. The relative imbalance in the Au + Au measurement with respect to d + Au reference is found to increase with the asymmetry of the trigger pair, consistent with the expectation from medium-induced energy-loss effects. In addition, this relative total transverse momentum imbalance is found to decrease for softer associated hadrons. Such evolution indicates that the energy missing at higher associated momenta is converted into softer hadrons.

I. INTRODUCTION

Angular di-hadron correlations with respect to a single charged or neutral high-p_T trigger at the center-of-mass energy per nucleon pair $\sqrt{s_{NN}} = 200$ GeV have been found to differ significantly between heavy-ion events and more vacuumlike pp or d + Au collisions. On the away side ($\Delta\phi \sim \pi$) of the trigger hadron, broader correlation distributions and softer transverse momentum (p_T) spectra of associated hadrons have been reported for central Au + Au events [1,2]. In some associated hadron p_T ranges ($\sim$2 GeV/c) the modified away side no longer resembles the jetlike peak but shows a concave shape near π. Novel features have also been discovered in Au + Au data on the near side (small relative azimuth) of the trigger hadron: a long-range longitudinal plateau in relative pseudorapidity ($\Delta\eta$), called the "ridge" [3]. Multiple theoretical models have been proposed to simultaneously explain these structures, including in-medium parton energy loss [4–9] and initial-state medium fluctuations leading to higher-order flow components such as the triangular flow (v_3) [10]. However, experimental measurements based on two-particle correlations with respect to high-p_T trigger introduce surface bias for the initial hard scattering. Thus, the partons and subsequently formed jets on the near and away sides can be affected by different underlying physics. However, di-hadron correlations between two high-p_T particles exhibit jetlike peaks in both near and away sides [11,12] with little shape modification from d + Au to central Au + Au, but a strong suppression on the away-side amplitude. This observation may be interpreted in two jet-medium interaction scenarios. One possibility is in-medium parton energy loss followed by in-vacuum fragmentation, which naturally explains the observed high-p_T inclusive hadron suppression, R_{AA}, defined as a ratio of spectra measured in Au + Au collisions with respect to binary-scaled pp reference [13,14]. Such a scenario can also explain little to no modifications of near-side peaks in the two-particle correlations (I_{AA}) [11,12]; however, lack of broadening on the away side of such correlation functions poses a challenge for this model [12]. Alternatively, there could be a finite probability for both partons to escape the medium without interactions. In the model this could be simplified as the "core/corona" model, where the dynamics of jets and di-jets in the medium are the same as in vacuum, unless they traverse the "core" of the medium where they are fully absorbed. In such scenario, the relative high-p_T per-trigger yield I_{AA} on the away side would be expected to be equal to the relative inclusive single high-p_T particle yield R_{AA}. Varying the surface bias experimentally could allow differentiating between the models.

The analysis presented in this paper uses a three-particle ("2 + 1") correlation technique for the data from

the Solenoidal Tracker at RHIC (STAR) [15]. A pair of back-to-back high-p_T trigger particles is used as proxies for the di-jet axis, and angular correlation of lower-p_T charged hadrons with respect to back-to-back trigger pair is considered. This technique was first introduced in the previous STAR publication [16]. In the early work, the primary trigger (T1) and its back-to-back secondary trigger partner (T2) had similar kinematic thresholds of ($p_T^{T1} > 5$ GeV/c and $p_T^{T2} > 4$ GeV/c). Following previous works, the near side is defined as the $\eta - \phi$ region close to trigger T1, and the away side is the $\eta - \phi$ space close to the away-side trigger T2. It has been found, that such di-jet-like correlations from central Au + Au collisions are similar in both shape and magnitude to those observed in d + Au events at the same incident energy on both near and away sides. This suggested a strong surface (tangential) bias of selected di-jets [16].

In this paper the analysis is further extended to higher primary trigger thresholds. We attempt to use the asymmetry in the energy of the two back-to-back triggers as a tool for changing the surface bias. The expectation is that such asymmetry can partially arise from a longer path length that the away-side parton must travel in the medium, thus producing differences in the balance of final jet energies. To control the degree of the surface bias we vary the relative balance between the energies of the primary trigger T1 (near side) and its back-to-back trigger partner T2 on the away side. For the most asymmetric trigger pair selection in this work the primary trigger has more than twice the energy of its back-to-back partner. The correlation functions and the spectra of associated charged particles around each trigger within $\Delta\phi < 0.5$ and $|\Delta\eta| < 0.5$ are measured and compared between Au + Au and d + Au reference data.

The total transverse momentum of each side of a di-jet is then calculated by summing the p_T for all associated charged hadrons plus the trigger E_T or p_T. The di-jet energy imbalance, $\Delta(\Sigma E_T)$, is calculated as the difference between the total transverse momentum between the same-side and away-side jetlike peaks. The absolute value of the imbalance could be affected by the kinematic selection of the trigger pair unrelated to the jet-medium interactions, for example, by the k_T effect. To provide quantitative assessment of jet-medium interaction effects and allow discriminating of the theoretical models, the relative di-jet energy imbalance between Au + Au and d + Au data is more informative.

II. DATA SETS

In this work the d + Au and Au + Au collisions at $\sqrt{s_{NN}} = 200$ GeV recorded by the STAR collaboration in Runs 2007 and 2008 are analyzed, extending analysis of

the previous, smaller, samples from Runs 2003 and 2004. Earlier measurement has been previously reported in Ref. [16]; we use these results here for comparison. The details of new datasets and analysis selections are discussed below. For a more uniform detector acceptance only events with a primary vertex position V_Z within 25 cm of the center of the STAR time projection chamber (TPC) along the longitudinal beam direction were used in the analysis. Run 2007 provided 74×10^6 Au + Au minimum-bias (MB) events. These MB events were selected by requiring at least one hit in the vertex position detectors (VPDs) located on each side of the TPC 4.5 m away from the nominal interaction point. A subset of such events with additional requirement of at least one high-energy tower (with transverse energy $E_T > 5.75$ GeV) in the barrel electromagnetic calorimeter (BEMC) is referred as the "high-tower trigger data." Run 2008 collisions provided 6×10^6 d + Au high-tower triggers (with $E_T > 4.3$ GeV) and 46×10^6 VPD minimum-bias triggered events. To maximize any medium effects, this work focuses on the analysis of 0%–20% most central Au + Au events.

The BEMC clusters are each built from a set of closely neighboring calorimeter towers and shower-max detector strips with appropriate shape and quality cuts. The BEMC cluster with the highest transverse energy of at least 8 GeV was selected as the primary trigger (T1). The triggered events were grouped into two different bins with $E_T \in [8, 10]$ GeV and $E_T \in [10, 15]$ GeV. A highest-p_T charge particle in the back-to-back azimuthal region ($|\phi^{T1} - \phi^{T2} - \pi| < 0.2$) is selected as the back-to-back partner trigger (T2) with kinematic requirement of $4 < p_T^{T2} < 10$ GeV/c. This width of 0.2 is an approximate width of the away-side peak in the high-p_T trigger-trigger correlation [11], ensuring a good balance between the di-jet purity and signal-to-background ratio. For proper primary trigger designation it is also required that the momentum of the secondary trigger is less than that of the primary one. The new data sets, especially benefiting from implementation of triggering capabilities of the STAR BEMC detector, allowed for significant improvement of the kinematic reach of this study, and thus larger asymmetry span in the back-to-back trigger partner selection. The primary trigger T1 threshold has been moved up by a factor of two while still maintaining a good energy resolution. The correlation is constructed with all other charged hadrons in an event. These associated particles are required to have transverse momentum $1.0 < p_T^{assoc} < 10$ GeV/c, and are divided into groups with different lower thresholds, [1, 10], [1.5, 10], [2, 10], and [2.5, 10] GeV/c. The kinematic selection for associated hadrons is intended to cover the region where the broadening of the away-side correlation and the near-side ridge were previously reported in the two-particle correlation measurements [1,3].

The associated charged particles reconstructed by TPC are required to pass a set of track quality cuts. Midrapidity $|\eta| < 1.0$ tracks selected are required to have at least 20 fit points for good momentum resolution, and a distance of closest approach (DCA) to the primary vertex of less than 1 cm. A fiducial cut of $|\eta| < 0.75$ is also required for the center of each EMC cluster. The high-p_T charged particle contamination in the BEMC trigger sample is removed by the following charged veto cut:

A BEMC-cluster trigger is rejected if a charged particle with $p_T > 1.5$ GeV/c is projected to a point within $|\Delta\phi| < 0.015$ and $|\Delta\eta| < 0.015$ of the center of the cluster.

III. ANALYSIS METHOD

A. Building the correlation functions

The correlation functions studied in this work are defined as

$$\frac{1}{N_{trig}} \frac{d^2N}{d\Delta\eta \, d\Delta\phi} = \frac{1}{N_{trig}\epsilon_{pair}} \left(\frac{d^2N_{raw}}{d\Delta\eta \, d\Delta\phi} \right) - a_{zyam} \frac{d^2N_{Bg}}{d\Delta\eta \, d\Delta\phi},$$

(1)

where N_{trig} is the number of trigger pairs, $d^2N_{raw}/d\Delta\eta \, d\Delta\phi$ is the associated hadron distribution relative to each trigger in correlated (T1, T2) pair, and ϵ_{pair} is a correction factor for single-track efficiency and pair acceptance effects. The $d^2N_{Bg}/d\Delta\eta \, d\Delta\phi$ represents a background term, originating predominantly from randomly associated pairs and correlations owing to anisotropic flow. Background scaling factor, a_{zyam}, is described in the text below. The tracking reconstruction efficiency is derived by embedding single Monte Carlo tracks into the real events and reconstructing the combined event. To account for the η, ϕ, p_T, and multiplicity dependence of the single-track reconstruction efficiency, the correction factor is calculated for each track individually and applied on a track-by-track basis. The pair acceptance correction is derived by the mixed-event technique. For the event mixing all accepted events with primary vertices $|V_Z| < 25$ cm are divided into ten 5-cm-wide bins. The events are also grouped into three centrality subclasses, corresponding to 0%–5%, 5%–10%, and 10%–20%. The triggers are then only mixed with associated particles from minimum bias events of the same V_Z and centrality bin to better reflect acceptance of real events and avoid potential trigger biases. Because the azimuthal acceptance of the STAR detector is uniform, the trigger pairs are used as a whole when mixing with minimum bias events, without the requirement for a correction to account for acceptance variations with respect to the second trigger direction alone. The two-dimensional ($\Delta\eta$-$\Delta\phi$) mixed-event correlation function is scaled such that the highest $\Delta\eta \sim 0$ bin is normalized to unity [see, e.g., Fig. 1(b)]. The raw correlation function (N_{raw}) is then divided by this normalized mixed-event distribution, shown in Fig. 1.

B. Background subtraction

The background term $\frac{d^2N_{Bg}}{d\Delta\eta d\Delta\phi}$ in Eq. (1) for each correlation function originates predominantly from random combinatorics and correlations induced by collective flow. The shape of this background is described by multiple components of a Fourier decomposition, with main contribution in the kinematic region of this analysis from the second-order Fourier component usually associated with elliptic flow (v_2). The multiplicity and p_T dependence of v_2 for triggers and associated particles are obtained from existing STAR measurements [17]. To reduce the effect of fluctuations in our v_2 estimate we average the results of event plane and four-particle cumulant methods [18].
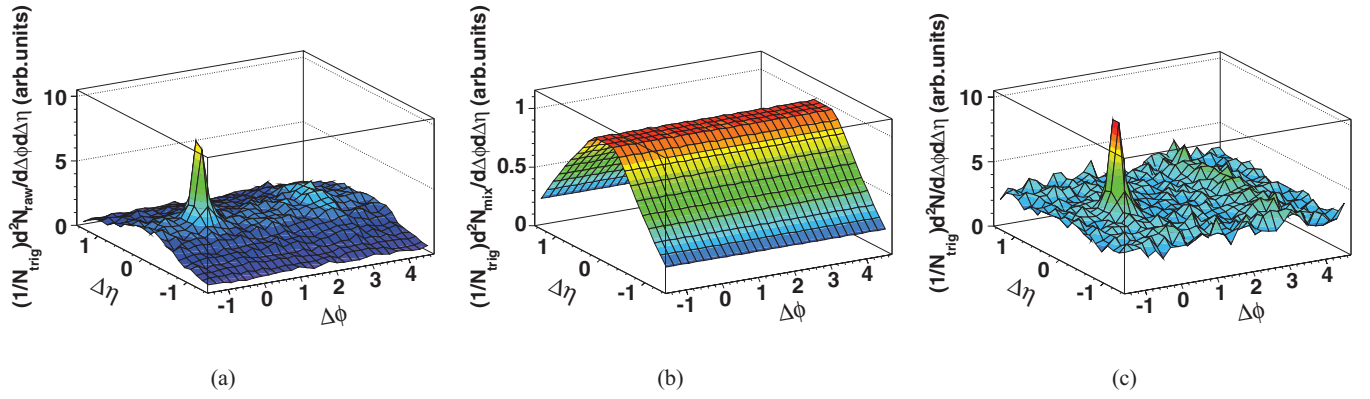
(a)　　　　　　　　　　　　　　　　(b)　　　　　　　　　　　　　　　　(c)

FIG. 1. (Color online) (a) A sample of two-dimensional raw correlation function from 200 GeV 0%–20% central Au + Au data before efficiency and acceptance correction. Primary trigger $E_T^{T1} \in [8,10]$ GeV, secondary trigger $p_T^{T2} \in [4,10]$ GeV/c, associated hadrons $1.5 \leqslant p_T^{assoc} \leqslant 10$ GeV/c. (b) Corresponding two-dimensional mixed-event pair-acceptance correction. (c) Same correlation function corrected for efficiency and pair acceptance effects.

For $p_T > 4$ GeV/c the elliptic flow magnitude is assumed to be constant and at the level reported in the high-p_T pion flow measurement [19]. This assumption is justified because the majority of charged hadrons at these momenta are charged pions [13,14], and high-E_T clusters used in this work are mainly produced by high-p_T π^0 [20]. Owing to the back-to-back requirement of trigger pair selection, the distribution (apart from efficiency and acceptance effects) is modulated by $f(\Delta\phi) = 1 + v_2^{2+1} \cos(2\Delta\phi)$, where v_2^{2+1} is the resulting flow modulation for three-particle correlation [21,22] given by

$$v_2^{2+1} = \frac{2v_2^{T1 \text{ or } T2} v_2^{assoc} + 2v_2^{T2 \text{ or } T1} v_2^{assoc} \frac{\sin(2\alpha)}{2\alpha}}{1 + 2v_2^{T1} v_2^{T2} \frac{\sin(2\alpha)}{2\alpha}}. \quad (2)$$

Here $\alpha = 0.2$ is the half width of the back-to-back trigger cone. The overall background level a_{zyam} is estimated with the zero-yield at minimum (ZYAM) method [23–25]. Each 2D correlation function within $|\Delta\eta| < 1.0$ is first projected on relative azimuth to optimize signal-to-noise ratio and avoid fluctuations at the edges of the TPC acceptance. Then the zero-yield region for the $2 + 1$ correlation is chosen to be consistently at least 1.3 rad away from both jetlike peaks at $\Delta\phi = 0$ or π. We note that this is more than 3σ of jetlike peak widths if fit by a Gaussian. A double Gaussian plus a

v_2-modulated background fit is also used for the background level estimate to evaluate systematic uncertainty of the ZYAM method. The transverse momentum spectra for associated hadrons in the jet peaks is obtained in a similar manner from the p_T-weighted correlations, selecting the hadrons within 0.5 rad in relative azimuth and 0.5 in relative pseudorapidity of the respective trigger direction.

An additional background term is related to the randomly associated triggers in the initial selection of the trigger pairs [23]. The signal-to-noise ratio is measured from the trigger-trigger correlation to estimate the relative contribution per trigger pair for such random associations. The correlation contribution owing to this background is constructed from two independent two-particle correlations for T1 and T2 trigger selections separately as in Ref. [16]. The ZYAM method is also applied to these two-particle correlations, and the zero-yield region is set to be [0.8, $\pi - 1.9$] relative to the trigger, also to avoid both jetlike peaks on near and away sides. An example trigger-trigger correlation to illustrate signal-to-noise ratio in trigger pairs is presented in Fig. 2(a). The dashed line shown in the figure illustrates the ZYAM level. The number of true di-jet triggers and random pairs is obtained from counting the entries above and below the ZYAM, respectively. The two-particle correlations used as estimates of correlated

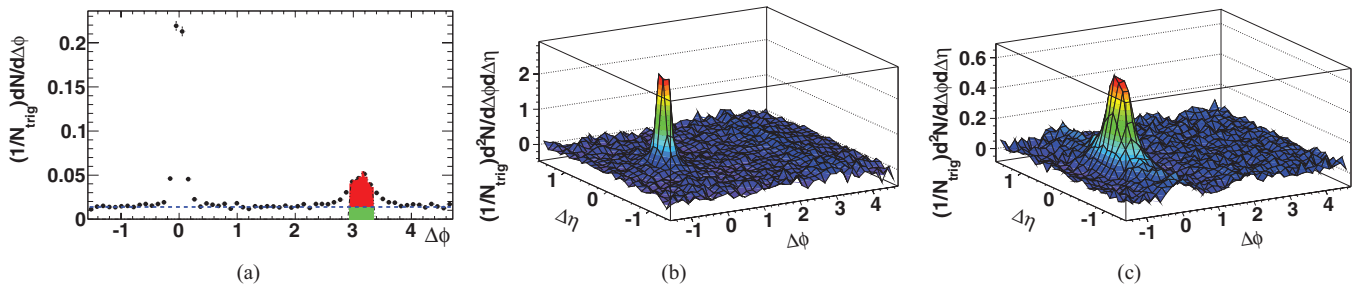(a)　　　　　　　　　　　　　　　　(b)　　　　　　　　　　　　　　　　(c)

FIG. 2. (Color online) (a) Azimuthal trigger-trigger correlation from 0%–20% central 200-GeV Au + Au collisions. Primary trigger $E_T^{T1} \in [8, 10]$ GeV, secondary trigger $p_T^{T2} \in [4, 10]$ GeV/c. The dashed line illustrates the ZYAM level. The contribution from randomly associated pairs for this analysis is visualized by the green area; that from true di-jets is visualized by the red one. (b) Di-hadron correlation for charged hadrons with $1.5 \leqslant p_T^{assoc} \leqslant 10$ GeV/c with respect to triggers matching T1 selection. (c) Di-hadron correlation for charged hadrons with $1.5 \leqslant p_T^{assoc} \leqslant 10$ GeV/c with respect to triggers matching T2 selection.
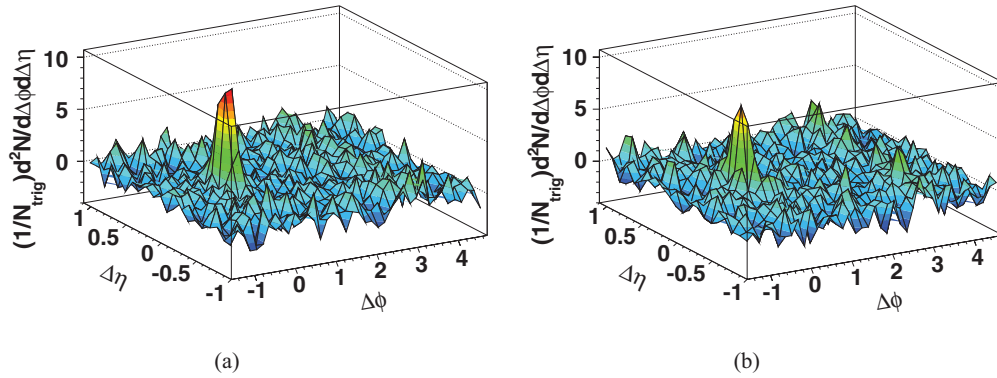
FIG. 3. (Color online) Fully corrected 2 + 1 correlation function from 0%–20% central Au + Au events with respect to the primary trigger (a) and secondary trigger (b). Primary trigger $E_T^{T1} \in [8, 10]$ GeV, secondary trigger $p_T^{T2} \in [4, 10]$ GeV/c, associated hadrons $1.5 \leqslant p_T^{\text{assoc}} \leqslant 10$ GeV/c.

background contribution corresponding to kinematic selection of first and second triggers are shown in Figs. 2(b) and 2(c), respectively. We note the known ridgelike structures evident in these two-particle correlations as expected.

A sample set of fully corrected 2 + 1 correlation functions is shown in Fig. 3, with the background induced by uncorrelated trigger pairs and the v_2 modulation removed. In the following sections we present all the correlation functions measured for the small relative angles only on both trigger sides to focus on the jetlike peaks.

An additional test was conducted to estimate possible effects from higher-order flow terms, such as v_3, on the correlations. This was done by including higher-order flow terms into the fit of final correlation functions such as in Fig. 3. We found the effects of v_3 to be negligible in the kinetic regime of this analysis. This result is reasonable as higher-order flow

terms are generally explained by the "soft" and "nonjet" sources; thus, the jet-dominant source of our trigger pairs could naturally lead to little or no v_3 contribution. Independent measurements [26] also confirm that the contributions from higher-order v_3 and v_4 terms are much smaller than v_2 in the trigger p_T region of this paper. Therefore, no corrections for flow terms other than v_2 are included in this analysis.

IV. RESULTS

A. Correlation functions and spectra

In this section we present results obtained from fully corrected correlations for each p_T bin studied for both d + Au and Au + Au datasets. The 2D correlations themselves are shown in Figs. 4–7 for primary triggers with transverse energy

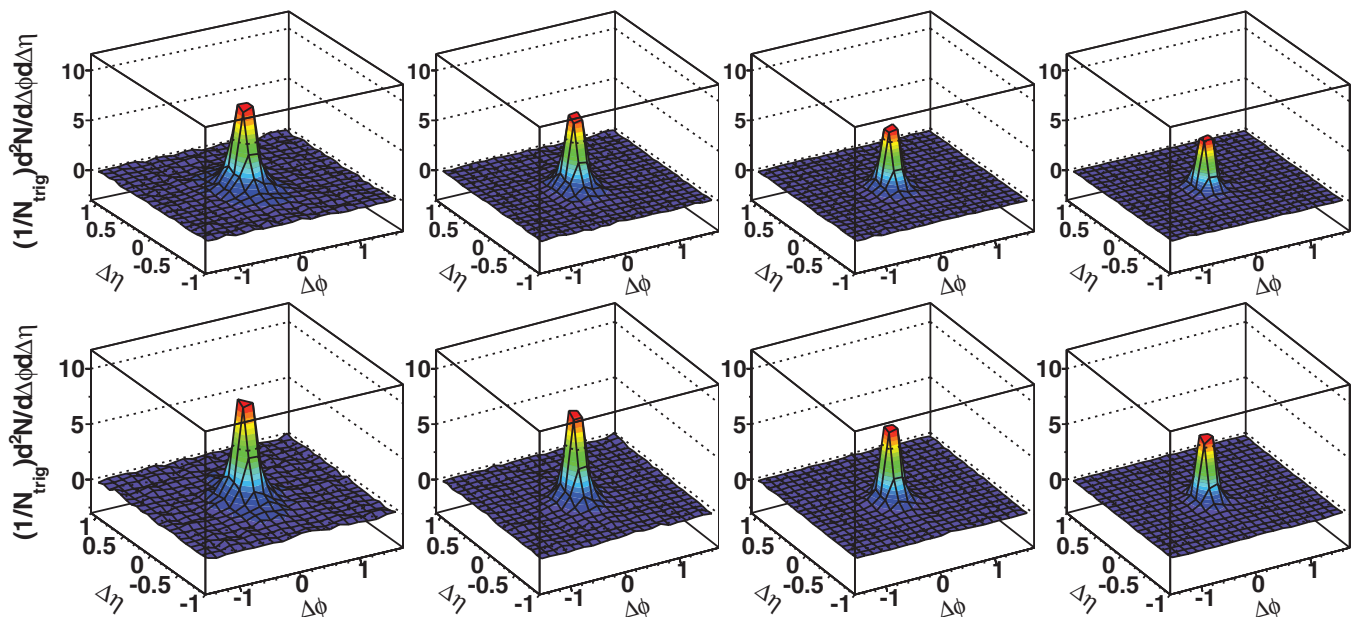
FIG. 4. (Color online) Near-side associated hadron distributions about primary triggers from 200-GeV d + Au data. The top row shows the correlations for the primary trigger E_T selection of [8,10] GeV; the bottom row shows that for [10,15] GeV. For all correlations the away-side trigger p_T is in [4,10] GeV/c. From left to right, the associated p_T ranges are [1,10] GeV/c, [1.5,10] GeV/c, [2,10] GeV/c, and [2.5,10] GeV/c.
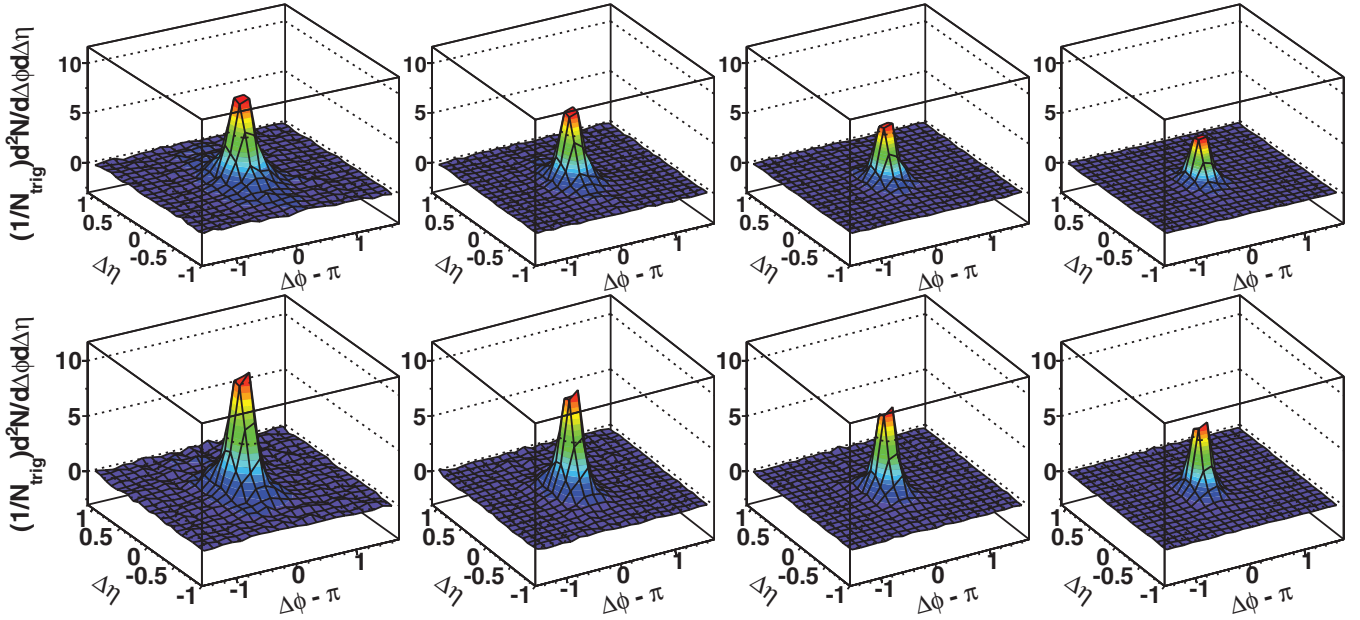
FIG. 5. (Color online) Away-side associated hadron distributions about secondary triggers from 200-GeV d + Au data. The top row shows the correlations for the near-side trigger E_T selection of [8,10] GeV; the bottom row shows that for [10,15] GeV. For all correlations the away-side trigger p_T is in [4,10] GeV/c. From left to right, the associated p_T ranges are [1,10] GeV/c, [1.5,10] GeV/c, [2,10] GeV/c, and [2.5,10] GeV/c.

$8 < E_T^{\mathrm{T1}} < 10$ GeV and $10 < E_T^{\mathrm{T1}} < 15$ GeV. The secondary back-to-back trigger for all correlations shown is chosen to have $4 < p_T^{\mathrm{T2}} < 10$ GeV/c. Only statistical errors are included in each of these plots.

In Figs. 8 and 9 the $\Delta\phi$ and $\Delta\eta$ projections of 2D correlation plots for the asymmetric back-to-back triggers studied are shown. The associated hadron transverse momentum selection for projections shown is [1,10] GeV/c, the lowest associated p_T bin studied. Also shown are the transverse momentum spectra for the associated charged particles within a 0.5×0.5 ($\Delta\eta \times \Delta\phi$) area of each trigger, the region containing the dominant part of the jetlike peak. Only statistical errors
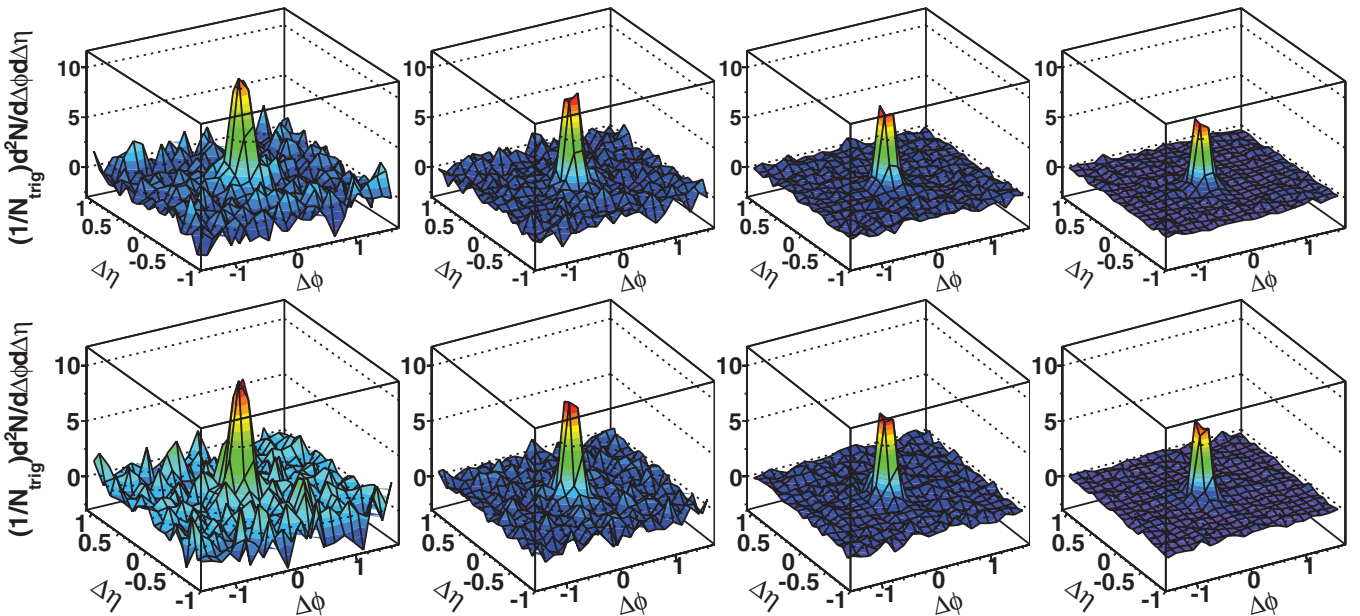

FIG. 6. (Color online) Near-side associated hadron distributions about primary triggers from 200-GeV 0%–20% central Au + Au data. The top row shows the correlations for the near-side trigger E_T selection of [8,10] GeV; the bottom row shows that for [10,15] GeV. For all correlations the away-side trigger p_T is in [4,10] GeV/c. From left to right, the associated p_T ranges are [1,10] GeV/c, [1.5,10] GeV/c, [2,10] GeV/c, and [2.5,10] GeV/c.
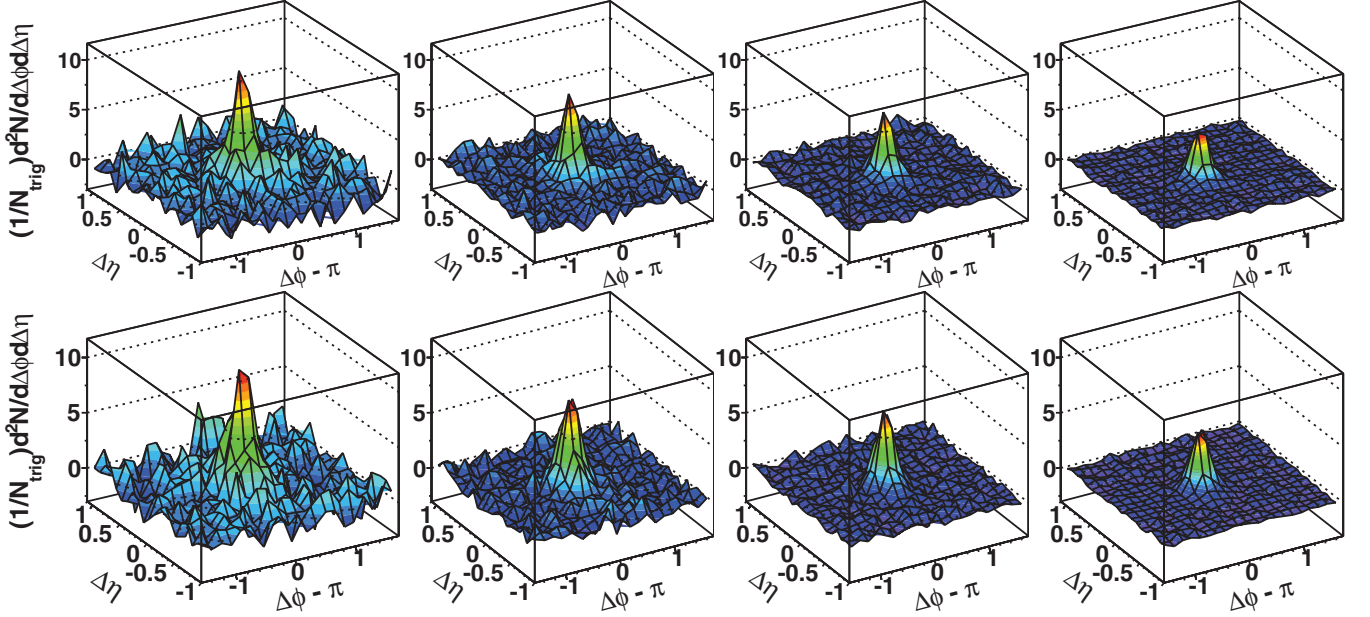
FIG. 7. (Color online) Away-side associated hadron distributions about secondary triggers from 200-GeV 0%–20% central Au + Au data. The top row shows the correlations for the away-side trigger E_T selection of [8,10] GeV; the bottom row shows that for [10,15] GeV. For all correlations the away-side trigger p_T is in [4,10] GeV/c. From left to right, the associated p_T ranges are [1,10] GeV/c, [1.5,10] GeV/c, [2,10] GeV/c, and [2.5,10] GeV/c.

are included in each of the plots; the systematic errors are strongly correlated between the near-/away-side signals of each collision system and are discussed in detail in the text. We find that for each T1 bin studied, the correlation functions and associated particle spectra from Au + Au events are similar to those observed in the d + Au data in spite of increased asymmetry between T1 and T2 triggers. The near-side yields of both the d + Au and the Au + Au data are smaller than their respective away-side yields, and the near-side Au + Au yield slightly drops when E_T of T1 increases from [8,10] to [10,15] GeV. Both observations are possibly attributable

to the increased direct γ contamination. This effect is further discussed later.

B. Systematic errors

Several sources of systematic uncertainties have been evaluated as outlined below. The single-track reconstruction efficiency for each centrality and p_T bin was derived as a 2D function of η and ϕ. The estimated uncertainty for this correction is 5% in each centrality-p_T-η-ϕ bin. This uncertainty is reduced to 1% when the correlated yields of the near side are
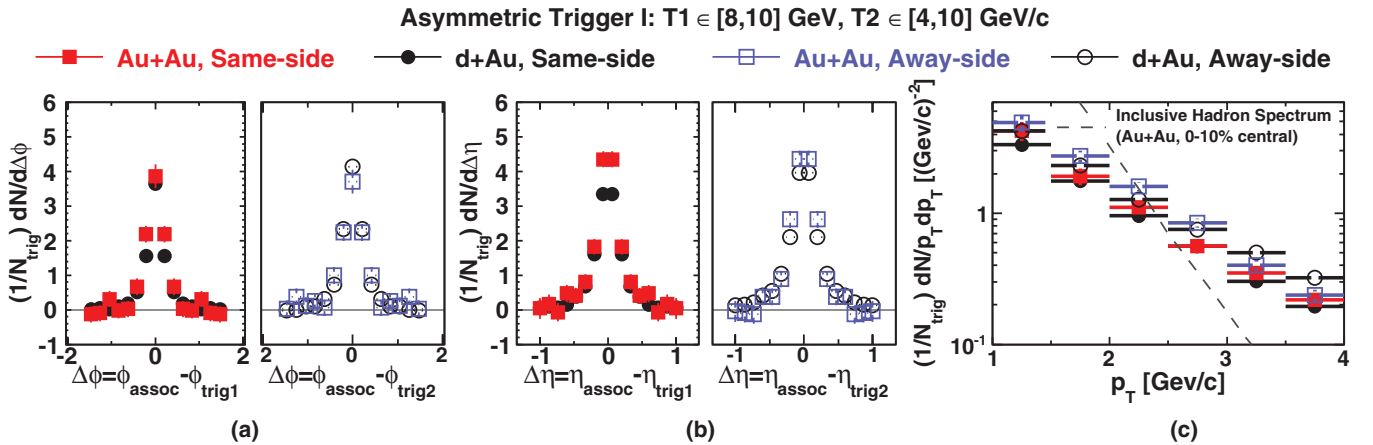

FIG. 8. (Color online) Projections of 2D correlation functions on $\Delta\phi$ (a) (with $|\Delta\eta| < 1.0$) and $\Delta\eta$ (b) (with $|\Delta\phi| < 0.7$) for the hadrons associated with their respective triggers (T1 for near side, T2 for away side) are shown for d + Au (circles) and central 0%–20% Au + Au (squares). Errors shown are statistical. The kinematic selection is as follows: $8 < E_T^{T1} < 10$ GeV, $4 < p_T^{T2} < 10$ GeV/c, $1.0 < p_T^{assoc} < 10$ GeV/c. (c) Transverse momentum spectral distributions per trigger pair for the near- and away-side hadrons associated with di-jet triggers ($|\Delta\phi| < 0.5$, $|\Delta\eta| < 0.5$). The inclusive charged hadron distribution from the central 0%–10% Au + Au data is shown for comparison.
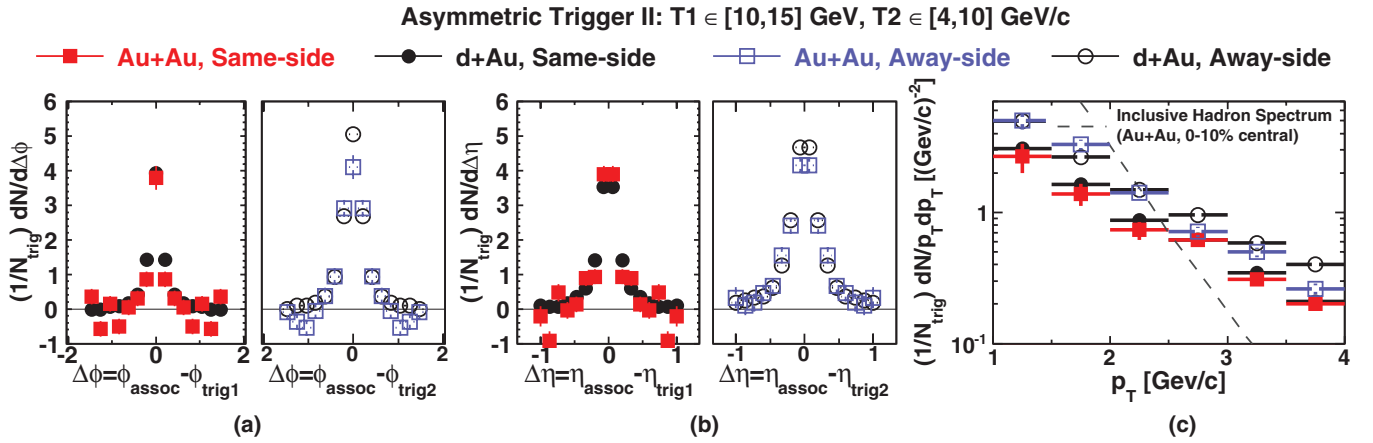
FIG. 9. (Color online) Projections of 2D correlation functions on $\Delta\phi$ (a) (with $|\Delta\eta| < 1.0$) and $\Delta\eta$ (b) (with $|\Delta\phi| < 0.7$) for the hadrons associated with their respective triggers (T1 for near side, T2 for away side) are shown for d + Au (circles) and central 0%–20% Au + Au (squares) data. Errors shown are statistical. The kinematic selection is as follows: $10 < E_T^{T1} < 15$ GeV, $4 < p_T^{T2} < 10$ GeV/c, $1.0 < p_T^{\rm assoc} < 10$ GeV/c. (c) Transverse momentum spectral distributions per trigger pair for the near- and away-side hadrons associated with di-jet triggers ($|\Delta\phi| < 0.5$, $|\Delta\eta| < 0.5$). The inclusive charged hadron distribution from the central 0%–10% Au + Au data sample is shown for comparison.

compared to those of the away side from the same data sample because the multiplicity-dependent effects cancel. The finite statistical uncertainty on the mixed-event correlation leads to a systematic uncertainty in the pair-acceptance correction. This error is estimated to be less than 5% for each centrality bin. The uncertainty owing to anisotropic flow contribution is estimated from the difference in the v_2 results from the event plane and four-particle cumulant methods. While the fluctuations of v_2 itself can be large, the final effect is relatively small owing to the evident jetlike peak shapes on both trigger sides. This uncertainty is found to be 5% in the central Au + Au. This uncertainty is largely correlated between the near and the away sides. It is not applicable to d + Au events where no v_2 modulation is included. Because higher-order Fourier terms, such as v_3 and v_4, have little effect on this analysis, no systematic uncertainties are assigned from these sources.

The systematic uncertainty owing to the ZYAM normalization of the background level was estimated by varying the $\Delta\phi$ range from which the minimum used in the ZYAM method was derived. Other background assumptions, such as a double-Gaussian plus v_2-modulated background are also used to estimate the scale of this uncertainty. The corresponding systematic uncertainty is found to be less than 5% in this analysis. This uncertainty is strongly correlated between near and away sides and cancels in relative side-to-side comparisons.

The systematic uncertainty owing to the correlated background subtraction from the di-jet sample is determined to be less than 3% for both d + Au and Au + Au events and is particularly small in the high-E_T trigger ranges where signal-to-background ratio is high. This error is also correlated between the near/away sides and is estimated by varying the background normalization for the trigger-trigger correlation in a manner similar to that used for the 2 + 1 correlation. Because two-particle correlations were used for the correction of random combinatorics of trigger pairs, the uncertainty in such di-hadron distributions arises mainly from the aforementioned

sources: uncertainty in v_2 and ZYAM normalization. These uncertainties were evaluated in a similar manner as above and the results are estimated to vary from less than 1% in d + Au events up to about 5% in central Au + Au data.

Despite the charged-veto cut, there are still possible contributions to the BEMC cluster trigger energy from low-p_T charged particles. This contribution is estimated via averaging the energy of those BEMC towers which are far from each trigger and pass the hot map cuts. The charged track signal contamination to the high energy tower cluster was estimated to be 2.5% in central Au + Au and less than 1% in d + Au.

The overall systematic uncertainty in each trigger-associated combination bin is less than 15% after all the contributions mentioned above are summed in quadrature. This is the level of uncertainties important for absolute measurements of the near-/away-side correlation functions or spectra in each collision system. The systematic errors are dominated by sources strongly correlated between near/away sides and will therefore mostly cancel when near and away sides are compared. Thus, relative measures, such as energy imbalance, have higher sensitivity to physics effects.

V. DISCUSSION

Our previous results [16] have shown similarity of the jetlike peaks not only on the near-side, but also on the away side of the primary high-p_T trigger between central Au + Au and d + Au data for the hadrons in the kinematic range of $p_T > 1.5$ GeV/c associated with the back-to-back high-p_T trigger pair. In addition, no evidence of the "dip" or "ridge" measured in di-hadron correlations with respect to a single trigger of similar kinematic selection is present in the 2 + 1 correlations reported in Ref. [16]. This similarity in the correlation shapes was further supported by the similarities in the associated hadron p_T distributions. Significant softening of the away-side spectra observed in di-hadron correlations [1], one of the

known indications of energy deposition into the medium, was not evident in these $2 + 1$ data. A simple accommodation for the observed differences between di-hadron and $2 + 1$ correlation results could be provided by the tangential di-jet emission scenario. In the presence of very strong energy loss in the core of the medium, only back-to-back parton pairs produced close to the surface and traversing the minimal amount of the medium could be recovered in the analysis. The Au + Au correlation functions would then naturally become similar to those of $d +$ Au. The $2 + 1$ results from symmetric triggers do not, however, exclude a path-length-dependent energy scenario, where finite in-medium energy loss is followed by in-vacuum fragmentation, for all di-jets. By increasing the asymmetry in transverse momentum between the two back-to-back trigger hadrons one may control the degree of the surface bias and thus the in-medium path length traversed by the parton. The path-length effects on energy loss then could be studied through the imbalance induced by the jet-medium interaction on the final energies of each side of a di-jet.

In this work the asymmetry between the back-to-back triggers is exceeding a factor of two; however, the correlations still show similar jetlike peak shapes and magnitudes from $d +$ Au to central Au + Au collisions for both the near and the away sides. No evident ridge or dip structure is observed at either near/away side in the Au + Au data. We point out that statistical limitations prevent the complete exclusion of a ridge [3], which could have a very small magnitude in the high-p_T trigger regime studied here. The absence of strong modifications in the Au + Au correlations relative to $d +$ Au signifies the intensity of jet-medium interactions, as the recovered di-jets still appear to have significant surface bias even for the large trigger asymmetry. We note an increase in the correlation magnitude on the away side with respect to the near side in both Au + Au and $d +$ Au correlations for our most asymmetric trigger pair selection. This increase by itself, as observed in both systems, is likely not related (or not in full) to the parton/jet energy loss. Because the trigger pairs preselected some di-jet asymmetry, the total yields and Σp_T of the associated particles from the higher-energy-trigger side must be lower owing to energy conservation without any energy loss. Hence, the relative change between Au + Au and the reference $d +$ Au data is a more relevant measure. Additionally, because the majority of the systematic errors are strongly correlated in this analysis between the near and

away sides, the measurements of relative differences also have an advantage from an experimental point. The spectra of associated charged particles for each trigger side from central Au + Au events are compared to the corresponding distributions from $d +$ Au data in Figs. 8 and 9. The ratios of Au + Au to $d +$ Au spectra are close to unity and have no prominent p_T dependence, indicating that the softening or suppression, if present, is not nearly as strong as observed in the single-particle R_{AA}.

An additional factor to consider in the comparisons is a possible direct-γ contamination of the primary triggers measured by BEMC clusters, because the near-side yields of direct-γ triggers are expected to be close to zero [27,28], potentially reducing the per-trigger measured yields on the near side. While the primary triggers from BEMC clusters of $8 < E_T^{\mathrm{T1}} < 15$ GeV are dominated by photon pairs from π^0 decays, grouped into the same BEMC cluster owing to large tower size, the direct γ contamination may not be negligible over the E_T range of this study [20]. We expect, however, that such direct-γ contamination would reduce the energy imbalance measured if it affected it at all: Because no in-medium energy loss is expected for direct γ, the away-side jet corresponding to such trigger would be relatively higher than that of π^0 trigger owing to the away-side (reverse) surface bias. Meanwhile, the consistent magnitudes of the near-side Au + Au and $d +$ Au correlation functions indicate that the contribution of direct-γ triggers is relatively small. In short, the $2 + 1$ correlations can be used as a tool for more differential measurements of path-length effects on in-medium energy loss for hard scattered partons.

The difference between the near- and away-side jet energy is used to quantify the medium effects. The jet energy is estimated by summing the E_T (p_T) of trigger and associated charged particles within the 0.5×0.5 ($\Delta\eta \times \Delta\phi$) area of each trigger in the kinematic range used in this analysis. The imbalance between the near and away sides is measured by the difference of the corresponding energy sums:

$$\Delta(\Sigma E_T) = \left(E_T^{\mathrm{T1}} + \Sigma p_T^{\mathrm{assoc,near}} \right) - \left(p_T^{\mathrm{T2}} + \Sigma p_T^{\mathrm{assoc,away}} \right).$$

This energy imbalance, $\Delta(\Sigma E_T)$, has smaller systematic uncertainty than energy sums for the correlated peaks themselves, as most sources of systematic errors cancel out as discussed above. A nonzero value of $\Delta(\Sigma E_T)$ could result from QGP medium effects and/or the known k_T effects characteristic for

TABLE I. Jet energy estimate for the near and away sides of back-to-back triggered correlations from 200-GeV $d +$ Au data. All units are in GeV or GeV/c. For both primary trigger selections listed, the secondary trigger is required to have transverse momentum $p_T \in [4, 10]$ GeV/c.

Trigger 1	$\langle E_T \rangle^{\mathrm{T1}}$ (GeV)	$\langle p_T \rangle^{\mathrm{T2}}$ (GeV/c)	Assoc p_T (GeV/c)	$\sum p_T^{\mathrm{assoc,near}}$ (GeV/c)	$\sum p_T^{\mathrm{assoc,away}}$ (GeV/c)	$\Delta(\Sigma E_T)$(GeV)
			[1.0,10.0]	4.09 ± 0.06	4.68 ± 0.06	2.74 ± 0.09
$E_T \in [8, 10]$ GeV	8.89	5.56	[1.5,10.0]	3.49 ± 0.06	3.94 ± 0.06	2.87 ± 0.08
			[2.0,10.0]	2.95 ± 0.06	3.26 ± 0.06	3.02 ± 0.08
			[2.5,10.0]	2.47 ± 0.06	2.62 ± 0.05	3.18 ± 0.08
			[1.0,10.0]	4.14 ± 0.07	5.75 ± 0.08	4.26 ± 0.11
$E_T \in [10, 15]$ GeV	11.74	5.86	[1.5,10.0]	3.59 ± 0.07	4.88 ± 0.08	4.58 ± 0.10
			[2.0,10.0]	3.09 ± 0.07	4.02 ± 0.07	4.95 ± 0.10
			[2.5,10.0]	2.65 ± 0.07	3.32 ± 0.07	5.20 ± 0.10

TABLE II. Jet energy estimate for the near and away sides of back-to-back triggered correlations from 200-GeV central Au + Au collisions. All units are in GeV or GeV/c. For both primary trigger selections listed, the secondary trigger is required to have transverse momentum $p_T \in [4, 10]$ GeV/c.

Trigger 1	$\langle E_T \rangle^{\text{T1}}$ (GeV)	$\langle p_T \rangle^{\text{T2}}$ (GeV/c)	Assoc p_T (GeV/c)	$\sum p_T^{\text{assoc,near}}$ (GeV/c)	$\sum p_T^{\text{assoc,away}}$ (GeV/c)	$\Delta(\Sigma E_T)$ (GeV)
			[1.0,10.0]	4.68 ± 0.27	4.82 ± 0.25	3.45 ± 0.37
$E_T \in [8, 10]$ GeV	8.87	5.27	[1.5,10.0]	3.81 ± 0.20	3.86 ± 0.17	3.55 ± 0.26
			[2.0,10.0]	3.16 ± 0.14	2.94 ± 0.12	3.82 ± 0.19
			[2.5,10.0]	2.61 ± 0.11	2.13 ± 0.09	4.08 ± 0.15
			[1.0,10.0]	4.12 ± 0.29	4.96 ± 0.24	5.21 ± 0.38
$E_T \in [10, 15]$ GeV	11.76	5.70	[1.5,10.0]	3.55 ± 0.21	4.00 ± 0.17	5.61 ± 0.26
			[2.0,10.0]	3.19 ± 0.14	3.10 ± 0.12	6.15 ± 0.19
			[2.5,10.0]	2.78 ± 0.11	2.27 ± 0.10	6.56 ± 0.15

back-to-back partons [29]. To disentangle these two contributions the measured energy imbalance for di-jets from central Au + Au events is compared with the corresponding value obtained from d + Au data with the same trigger/associated particle p_T cuts. The energy imbalance for symmetric trigger pairs [16] was found to be 1.59 ± 0.19 GeV/c in central Au + Au collisions, similar to the value of 1.65 ± 0.39 GeV/c reported for the minimum bias d + Au data. This value is also close to the initial-state k_T effects of ~ 1.6 GeV/c estimated in di-jet correlation [9] and disfavors additional partonic energy loss into the medium for these Au + Au data. The detailed results for our new measurement for the asymmetric trigger pairs are summarized in Tables I and II. In each table, only the statistical uncertainties are listed for each variable. The statistical uncertainties on mean values of trigger E_T or p_T are negligible.

In Fig. 10 the relative energy imbalance between central Au + Au and d + Au data [e.g., $\Delta(\Sigma E_T)^{\text{Au+Au}} - \Delta(\Sigma E_T)^{d+\text{Au}}$] is shown for both the symmetric (solid symbol) and asymmetric trigger cases (open symbols). The errors shown include both statistical and systematic uncertainties discussed in the previous section.
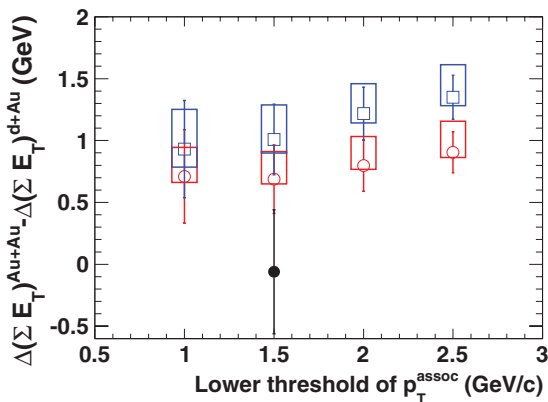

FIG. 10. (Color online) The relative di-jet energy imbalance estimate $\Delta(\Sigma E_T)^{\text{Au+Au}} - \Delta(\Sigma E_T)^{d+\text{Au}}$. The open circles show results for primary triggers in [8,10] GeV; the open squares show that for [10,15] GeV. The solid data point is the result for symmetric trigger pairs from previous STAR paper [16]. The x axis shows the lower threshold of the transverse momentum selection for associated hadrons.

The observed relative energy imbalance $\Delta(\Sigma E_T)^{\text{Au+Au}} - \Delta(\Sigma E_T)^{d+\text{Au}}$ between Au + Au and d + Au for the asymmetric trigger pairs studied is consistent with nonzero values. The relative imbalance is consistently higher for all associated hadron selections for more asymmetric triggers, as expected if larger asymmetries are related to longer paths traversed and higher energy loss. The measured values of relative energy imbalance are significantly smaller than the theoretical prediction for in-medium energy deposition based on path-dependent energy loss [9]. In this model approximately 3 GeV is expected for our asymmetric case. The $2 + 1$ results for both symmetric and asymmetric trigger pairs seem to favor much stronger surface bias than expected in theory and thus point to stronger path-length dependence of energy loss. Also, as previously discussed, any direct-γ contamination to our primary trigger sample would reduce the observed energy imbalance, leading to even greater discrepancy between the data and the theory. We note, however, that if part of the energy deposited to the medium by the traversing parton produces hadrons that remain within the angular selection of our jet peaks, it will not be observed in the relative imbalance variable. Thus, it is possible that we only measure part of the lost energy that got redistributed to hadrons that are softer than those considered in this study, or that were radiated at larger angles than those included in our jet-cone selection. The dependence of observed energy imbalance on the associated hadron p_T seems to confirm this idea. The relative imbalance is found largest for the highest associated hadron p_T bin studied, reaching the value ~ 1.5 GeV/c, and decreasing for the softer associated hadrons to approximately ~ 1 GeV/c. This trend can indicate that the jet fragmentation is shifted to the lower-p_T regime (softening), or that the lower-energy fragmentation products are at larger angles from the jet axis (broadening). The later is less likely attributable to consistent jetlike peak widths observed in Au + Au and d + Au events. In either of the two cases, in the limit of associated hadron p_T approaching zero, the value of relative $\Delta(\Sigma E_T)^{\text{Au+Au}} - \Delta(\Sigma E_T)^{d+\text{Au}}$ consistent with zero would indicate that full jet energy is recovered. Extrapolating our data to very low momenta, albeit large uncertainties, seems consistent with this scenario.

Additional information could be obtained from the relative di-jet production rates. For the surface-emission scenario the jets and di-jets production rates are determined by the surface
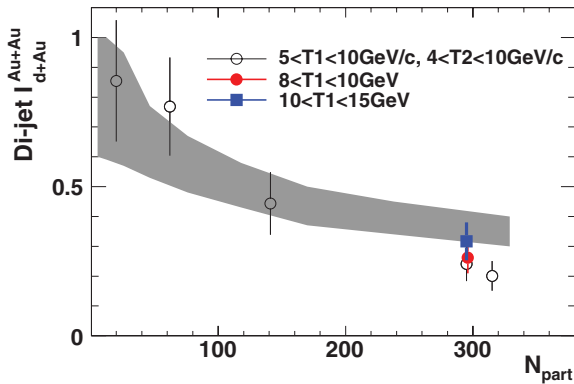
FIG. 11. (Color online) Conditional di-jet survival probability measured through di-jet relative suppression rates I_{d+Au}^{Au+Au} as a function of centrality. The circles show data from Ref. [16]. Solid symbols show new measured ratios for the asymmetric trigger pairs with primary triggers of [8,10] GeV and [10,15] GeV. The band shows the expectation for di-jet surface emission ("corona" only) rates from Ref. [16].

volume of the fireball. In simplest implementation of this scenario the medium in heavy-ion collisions is modeled consisting of a completely opaque core (leading to full jet absorption) surrounded by a permeable corona (with no jet-medium interactions). In such a model a parton (jet) will survive with no energy loss or modifications if the underlying hard-scattering happened in the corona region and the scattered parton did not pass through the core. A Monte Carlo Glauber model based on such a model was compared to the early di-jet production rates in Ref. [16]. The size of the permeable corona was first determined from tuning to the measured single charged hadron R_{AA} results from RHIC. It was then used to predict the di-jet survival probability for the back-to-back triggers. To minimize systematic uncertainties related to the determination of the number of binary collisions (N_{coll}) and the number of participating nucleons (N_{part}) in the Glauber model, the double ratios measuring conditional di-jet survival probability were used. Such a double ratio, $I_{d+Au}^{Au+Au} = \frac{R_{AA}^{di\text{-}jet\ triggers}}{R_{AA}^{single\ triggers}}$, constructed from nuclear modification factors (R_{AA}, the binary scaled ratios of the observables in Au + Au and d + Au collisions), reflects any changes in probability to find an away-side trigger for each primary trigger observed in Au + Au data relative to d + Au. In the earlier work the value $I_{d+Au}^{Au+Au} = 0.20 \pm 0.05$ for the symmetric trigger pairs was found to be qualitatively consistent with the estimates of a simplistic core/corona model [16]. The di-jet survival probability was calculated the same way in this work for the new asymmetric trigger data. These additional new points for the 0%–20% central Au + Au data are included in Fig. 11, which reproduces the plot from the previous work. We find the conditional survival rate I_{d+Au}^{Au+Au} for the asymmetric trigger pairs to be 0.26 ± 0.05 for $E_T^{T1} \in [8, 10]$ GeV and 0.32 ± 0.06 for $E_T^{T1} \in [10, 15]$ GeV. We note that the dominant source of systematic uncertainties comes from N_{bin} calculation in the Glauber model, which is then fully correlated between the data points of the same centrality bin (new values) and largely correlated between the values for central collisions between the data from different

runs. So the slight increase in di-jet conditional survival with increasing trigger pair asymmetry points to higher in-medium path lengths, which is consistent with our conclusions based on the relative energy imbalance. In other words, the new values of I_{d+Au}^{Au+Au} indicate that jets triggered by those more asymmetric back-to-back pairs are emerging from deeper within the "core" of the medium compared to a more symmetric pair selection.

VI. SUMMARY

Jet-medium interactions were studied via a $2 + 1$ multi-hadron correlation technique. For both symmetric and asymmetric trigger pairs, the distributions of associated hadrons and their spectra show no strong shape modifications from d + Au to central Au + Au collisions on both near- and away-trigger sides. This is in contrast to the di-hadron correlation results with respect to a single high-p_T trigger. In addition, no evidence of the near-side "ridge" [3] or the away-side "shoulders" [2] was observed in these $2 + 1$ correlations. The relative total transverse momentum imbalance was measured as an excess in the difference between the sum of the momentum (or energy) for hadrons attributed to the near-side and away-side jetlike peaks in Au + Au with respect to the reference d + Au data. The relative imbalance of Au + Au over d + Au has been shown to be nonzero for the asymmetric trigger pair selections and increasing with the asymmetry of the trigger pair. This is consistent with expected medium effects for partons probing deeper within the medium. This challenges the simplistic implementation of the full absorption "core/corona" model, which captured well the centrality trend of di-jet production rates for the symmetric triggers. The relative imbalance is found largest for the highest associated hadron p_T bin studied, reaching the value $\sim$1.5 GeV/c, and decreasing for the softer associated hadrons. This trend indicates that the energy missing from the away-side peak at higher associated momenta is converted into softer hadrons. The measured relative imbalance for all bins is less than the theoretical predictions for total in-medium energy deposition for such trigger pairs of $\sim$3 GeV/c in the path-length-dependent energy-loss model [9]. We note, however, that if part of energy deposited to the medium by the traversing parton produces hadrons that remain within the angular selection of our jet peaks, it will not be observed in the relative imbalance variable.

[1] J. Adams *et al.*, Phys. Rev. Lett. **95**, 152301 (2005).
[2] A. Adare *et al.*, Phys. Rev. C **78**, 014901 (2008).
[3] B. Abelev *et al.*, Phys. Rev. C **80**, 064912 (2009).
[4] P. Arnold, G. D. Moore, and L. G. Yaffe, J. High Energy Phys. 11 (2001) 057.
[5] X.-N. Wang and X. Guo, Nucl. Phys. A **696**, 788 (2001).
[6] C. A. Salgado and U. A. Wiedemann, Phys. Rev. D **68**, 014008 (2003).
[7] I. Vitev, Phys. Lett. B **630**, 78 (2005).
[8] A. D. Polosa and C. A. Salgado, Phys. Rev. C **75**, 041901 (2007).
[9] T. Renk, Phys. Rev. C **78**, 014903 (2008).
[10] G.-Y. Qin, H. Petersen, S. A. Bass, and B. Muller, Phys. Rev. C **82**, 064903 (2010).
[11] J. Adams *et al.*, Phys. Rev. Lett. **97**, 162301 (2006).
[12] A. Adare *et al.*, Phys. Rev. Lett. **104**, 252301 (2010).
[13] J. Adams *et al.*, Phys. Rev. Lett. **91**, 172302 (2003).
[14] S. S. Adler *et al.*, Phys. Rev. Lett. **91**, 072301 (2003).

[15] K. H. Ackermann *et al.*, Nucl. Instrum. Methods Phys. Res., Sect. A **499**, 624 (2003).
[16] H. Agakishiev *et al.*, Phys. Rev. C **83**, 061901 (2011).
[17] J. Adams *et al.*, Phys. Rev. C **72**, 014904 (2005).
[18] C. Pruneau, S. Gavin, and S. Voloshin, Nucl. Phys. A **802**, 107 (2008).
[19] A. Adare *et al.*, Phys. Rev. Lett. **105**, 142301 (2010).
[20] S. S. Adler *et al.*, Phys. Rev. Lett. **94**, 232301 (2005).
[21] J. Ulery and F. Wang, Nucl. Instrum. Methods Phys. Res., Sect. A **595**, 502 (2008).
[22] J. Bielcikova, S. Esumi, K. Filimonov, S. Voloshin, and J. P. Wurm, Phys. Rev. C **69**, 021901 (2004).
[23] B. Abelev *et al.*, Phys. Rev. Lett. **102**, 052302 (2009).
[24] C. Adler *et al.*, Phys. Rev. Lett. **90**, 082302 (2003).
[25] A. Adare *et al.*, Phys. Rev. Lett. **98**, 232302 (2006).
[26] A. Adare *et al.*, Phys. Rev. Lett. **107**, 252301 (2011).
[27] A. Adare *et al.*, Phys. Rev. D **82**, 072001 (2010).
[28] B. Abelev *et al.*, Phys. Rev. C **82**, 34909 (2010).
[29] S. S. Adler *et al.*, Phys. Rev. D **74**, 072002 (2006).